Robustness Analysis of Direct and Indirect RFOC under Parameter Variations for E-Taxiing

Rokhaya SOW[1,2] Zohra KADER[1] Stephane CAUX[1]

Maurice FADEL[1] Wenceslas BOURSE[2] Frédéric BACH[2]

Abstract – Induction motors (IM), known for their robustness, simplicity, and low maintenance, are widely used in various fields, especially in traction applications. They are also employed in aerospace applications due to their reliability and performance in demanding environments. Field-oriented control (FOC) techniques, specifically Rotor FOC (RFOC), are employed as advanced control strategies to achieve high dynamic performance and accurate torque control. This paper first compares direct RFOC (DRFOC) and indirect RFOC (IRFOC) strategies. Given the increasing adoption of speed sensorless control schemes in modern applications, this study incorporates a sensorless speed control approach alongside DRFOC, using a extended Kalman filter to estimate rotor flux and motor speed. Then, considering the practical for ground airplane traction (e-taxiing), the impact of unavoidable parameter variations is also taken into account. In order to predict the accuracy of the control torque following parameter changes, a theoretical analysis of the impact on the IRFOC control strategy is performed.

Keywords – More electric aircraft (MEA), e-Taxiing, Induction motor, direct and indirect rotor field oriented control (DRFOC, IRFOC), extended Kalman filter, prediction of torque accuracy

1. INTRODUCTION

In a global context driven by the emergency to reduce greenhouse gas emissions and accelerate the energy transition, the aviation sector faces unprecedented challenges. Among these challenges, the decarbonization [1] has become a central priority [2]. Electrification of propulsion systems for aircraft presents a compelling solution, enabling significant reductions in pollutant emissions while enhancing energy efficiency, reliability, and overall performance. The changes that will be considered under the MEA (More Electric Aircraft) are summarized in the table (1) below. The work will focus on the section related to the Electric Ground Traction [3]. A set of studies has been conducted with the aim of comparing electric motors and selecting the most suitable one based on the objective. Following a large comparative test (thermal, mechanical, and electrical) and a study on the safety related aspects specific to the application, the squirrel-cage induction motor was chosen. The development of more electric propulsion systems thus represents a crucial step toward sustainable aviation, aligning technological innovation with pressing environmental imperatives.

However, this transition presents significant technological challenges, particularly the development of control systems designed to ensure precise operation under conditions of high torque and/or high-speed demands.

Advanced control techniques, such as Direct Self Control (DSC)[5], Direct Torque Control (DTC) have been proposed [4] but one, Field-Oriented Control (FOC) [6], stands out for its accuracy and rapidity during transient periods. It plays a critical role and ensure a good torque and speed regulation for aeronautical applications. These methodologies address stringent performance and robustness requirements while minimizing energy losses. FOC can be implemented using two control methods : Indirect and Direct (IRFOC, DRFOC). The first relies mathematical models and motor parameters, such as rotor resistance and rotor inductance (slip frequency), to indirectly estimate the rotor flux position. Whereas, the second one is more complex as it directly utilizes the rotor flux, requiring a flux estimator [11]. This study aims to evaluate how combined variations in machine parameters, specifically rotor resistance (R_r) and mutual inductance (L_m), affect the torque regulation of the machine across various operating points under two control strategies. A particular focus is placed on the indirect control method, where an analytical relationship is proposed to directly link the estimation error of the transformation angle θ_e to the error in the generated torque. This work seeks to provide clear insights into the impact of parameter variations on the performance and accuracy of torque control.

This article is organized as follows: Section 2 provides the context, emphasizing the challenges associated with the application. Next, the principles of rotor field-oriented control is explored, highlighting the distinction between direct and indirect methods, as well as their implementation challenges. Section 4 presents a theoretical analysis of the effects of parametric variations, examining how changes in motor parameters impact system performance and control accuracy. Finally, simulation results are presented to validate the theoretical findings.

Table 1. Comparison between Conventional Aircraft and MEA

Conventional Aircraft	**MEA (More Electric Aircraft)**
Conventional engine, generates hydraulic, pneumatic and electric power; pneumatic start-up	Bleed-less or less bleed engine, electric start-up
Conventional APU, generates hydraulic, pneumatic and electric power	Electrical APU, only generates electric power
A few power electronics converters	More power electronics converters
Hydraulic and pneumatic actuators (HA & MA)	More Electric actuators (EHA & EMA)
Hydraulic brakes	Electric brakes
AC circuit breakers and low voltage DC breakers	More Solid state power contactors (SSPCs)
Battery only used in emergency condition and for APU start-up	Used in all flight phases
Conventional traction with engine and tugs	Electric Ground Traction (e-Taxiing)

[1] firstName.lastName@laplace.univ-tlse.fr, LAPLACE, Université de Toulouse, CNRS, INPT, UPS, Toulouse, France

[2] firstName.lastName@safrangroup.com, Safran Landing Systems and Safran Ventilation Systems, Paris and Toulouse, France.

2. STUDY CONTEXT

This work is part of the development of a more electric traction system for aircraft, aiming to contribute to aviation decarbonization. The 'e-Taxiing' electric taxiing system enables aircraft to move on the ground, positioning them for takeoff preparation or assisting them in reaching the airport area after landing (Figure 1).

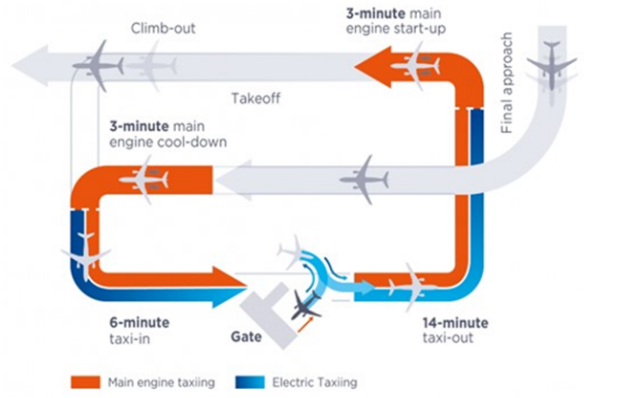

Figure 1. Layout of the e-Taxiing System Circuit

Figure 2 shows the typical motor profile used in the taxiing system. Point **P1** (maximum torque) marks the breakaway point, representing the minimum torque required to overcome friction and initiate the aircraft's motion. From point **P2** (base speed) onwards, the system operates in the constant power region, where both flux (due to field weakening) and torque vary. Point **P7** indicates the maximum speed point, while points **P3, P6,** and **P8** correspond to the test points used in the simulations. Furthermore, in most cases, the equipment will be controlled by torque rather than speed, making torque precision crucial.

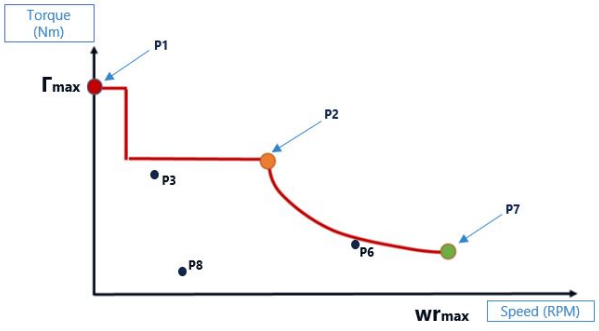

Figure 2. Speed torque profil

Based on this profile, the application requires the system to operate at either high speed or high torque. During operation, variations in resistances (R_s, R_r) occur due to motor aging or significant temperature changes. These variations depend also on the operating point (influenced by fluctuations in stator and rotor currents) and the environment, where temperatures can range from -40°C to 150°C. Similarly, variations in inductance (L_m) may arise, driven by changes in the desired operating points (such as in the field weakening region) and temperature.

One of the key challenges is designing a robust control system capable of handling these parameter variations, as they can significantly impact the system's performance. Such variations can lead to inaccuracies in estimating critical parameters, such as current references and slip frequency, which are essential for precise control in RFOC methods. As a result, these fluctuations may degrade performance, reduce efficiency, or, in extreme cases, cause instability.

Given these considerations, this paper presents an analytical study exploring how parameter fluctuations impact the torque generated by the motor and proposes possible solutions to address this issue.

3. ROTOR FIELD ORIENTED CONTROL

Field-Oriented Control (FOC), also known as vector control, is an advanced method for controlling electric machines by transforming three-phase quantities (a, b, c) into an orthogonal reference frame (d, q) aligned with the magnetic field. The angle θ_e, representing the position between the reference armature coil (as) and axe (d) of reference frames, is critical for accurately projecting the electrical quantities.

For the RFOC, the (d, q) reference frame is aligned with the rotor flux ψ_r, as shown in Figure 3.

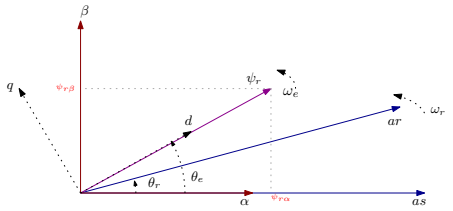

Figure 3. Vectorial representation of the dq axis orientation.

Thus, with $\psi_{rq} = 0$ and $\psi_{rd} = \psi_r$, the electromagnetic torque equation is simplified :

$$\Gamma_{em} = \frac{3}{2}.n_{pp}.\frac{L_m}{L_r}.\psi_{rd}.i_{sq} \tag{1}$$

The expression of the flux is :

$$\psi_{r_d} = \frac{R_r.L_m}{R_r + p.L_r}.i_{s_d} \tag{2}$$

It can be observed that, in the (d, q) reference frame with constant flux, the control of torque and flux is decoupled. Torque is controlled by the quadrature stator current, while flux is controlled by the direct stator current. This is the fundamental basis of vector control.

The internal control loop of the system (Figure 4) is based on the following equations (3), [7] :

$$\begin{cases} v_{sd} = R_{eq}.i_{sd} + L_{eq}.p.i_{sd} + E_d \\ v_{sq} = R_{eq}.i_{sq} + L_{eq}.p.i_{sq} + E_q \end{cases} \tag{3}$$

with

$$R_{eq} = R_s + R_r.\frac{L_m^2}{L_r^2}$$

$$L_{eq} = \sigma.L_s$$

$$E_d = -\omega_e\,\sigma L_s i_{sq} - R_r\frac{L_m}{L_r^2}\psi_{rd} \qquad E_q = \omega_e\,\sigma L_s i_{sd} + \omega_r\frac{L_m}{L_r}\psi_{rd}$$

$$L_s = L_{ls} + L_m \;\; and \;\; L_r = L_{lr} + L_m$$

Where, "p" is the Laplace operator R_s and R_r represent the stator and rotor resistances, L_{l_s} and L_{l_r} are the stator and rotor leakage inductances and L_m corresponds to the mutual inductance. ω_r represents the electrical pulsation, ω_e is synchronous pulsation and Γ_{em} refers to the electromagnetic torque. The number of pole pairs is represented by n_{pp}.

$._{sd}$ and $._{sq}$ refer to the direct and quadrature stator quantities, with the symbol "." representing either "i" (current), "v" (voltage), or "ψ" (flux) respectively.

The DRFOC and IRFOC are used depending on the method applied to determine the transformation angle θ_e.

3.1. *Direct RFOC*

For this technique, θ_e is obtained directly from the projection of the flux onto the stationary α-β frame. From this, the angle is given by

$$\theta_e = tan^{-1}(\frac{\psi_{r\beta}}{\psi_{r\alpha}}), \tag{4}$$

with, ψ_{r_α} and ψ_{r_β} are the rotor flux coordinates in the stationary frame.

3.2. *Indirect RFOC*

In contrast to the direct method, this approach determines the transformation angle θ_e based on the slip angular velocity ω_{sl}. This method requires less complex equations and reduces computational time compared to the DRFOC method.

4. ESTIMATION OF θ_e FOR DRFOC AND IRFOC CONTROL

4.1. *DRFOC θ_e estimation : Kalman Observer*

The complexity of the Direct RFOC arise from the absence of a flux sensor, which requires the flux to be estimated or observed. In this case, the rotor flux is estimated using Extended Kalman Filters (EKF). The discrete form of the system is :

$$x_{k+1} = A_d(x_k) \cdot x_k + B_d \cdot u_k + w_k; \quad y(k) = C_k \cdot x_k + v_k$$

w_k and v_k are, respectively, the process and measurement noises.
The general algorithm of the filter is defined in this paper [10].

For the case of induction machine, to design the observer, the (α, β) model is used, which is the (d, q) reference in the stationary frame.

State vector :

$$x_k = \begin{bmatrix} i_{s_\alpha}(k) & i_{s_\beta}(k) & \psi_{r_\alpha}(k) & \psi_{r_\beta}(k) & w_r(k) & \Gamma_{Load} \end{bmatrix}.$$

$w_r(k)$, the 5th component observed, because it assumes that the system is speed sensorless.
$y(k)$ = [$i_{s_\alpha}(k)$ $i_{s_\beta}(k)$] represents the measured currents, and the control input vector is u_k = [$v_{s_\alpha}(k)$ $v_{s_\beta}(k)$], which refers to the stator voltages measured in the stationary frame.
B_d is defined as the discretized input matrix and C is the measurement matrix. Given that only the currents are measurable.
Below is the machine model in the stationary $\alpha\beta$ reference frame.
The following is a matrix representation of the system, [9] :

$$\tau_r = \frac{L_r}{R_r},\ \sigma = 1 - \frac{L_m^2}{L_s.L_r},\ a_{11} = \frac{R_s}{\sigma.L_s} + \frac{1-\sigma}{\sigma.\tau_r},\ a_{13} = \frac{L_m}{\sigma.L_s.L_r.\tau_r},\ a_{14} = a_{13}.\tau_r,\ a_{31} = \frac{L_m}{\tau_r},\ b_{11} = \frac{1}{\sigma.L_s}$$

$$A_{d_5} = \begin{bmatrix} 1 - T_e \cdot a_{11} & 0 & T_e \cdot a_{13} & T_e \cdot a_{14} & 0 \\ 0 & 1 - T_e \cdot a_{11} & -T_e \cdot a_{14} \cdot \omega_r(k) & T_e \cdot a_{13} & 0 \\ T_e \cdot a_{31} & 0 & 1 - T_e \cdot \frac{1}{\tau_r} & -T_e \cdot \omega_r(k) & 0 \\ 0 & T_e \cdot a_{31} & T_e \cdot \omega_r(k) & 1 - T_e \cdot \frac{1}{\tau_r} & 0 \\ 0 & 0 & 0 & 0 & 1 \end{bmatrix}$$

$$B_{d_5} = \begin{bmatrix} T_e b_{11} & 0 & 0 & 0 & 0 \\ 0 & T_e b_{11} & 0 & 0 & 0 \end{bmatrix}^t \qquad C_5 = \begin{bmatrix} 1 & 0 & 0 & 0 & 0 \\ 0 & 1 & 0 & 0 & 0 \end{bmatrix}$$

$X_{(i:j,k:l)}$ is the submatrix's extraction of matrix X defined by rows from i to j and columns from k to l.

$$A_{d_6} = \begin{bmatrix} A_{d_5\,(1:4,1:4)} & \begin{bmatrix} 0 & 0 & 0 & 0 \\ 0 & 0 & 0 & 0 \end{bmatrix}^t \\ A_{d_{6_{(5:6)}}} & \begin{bmatrix} -T_e \cdot \frac{n_{pp}}{J} & 1 \end{bmatrix}^t \end{bmatrix}$$

where,

$$A_{6_{(5:6)}} = \begin{bmatrix} -T_e \cdot a_{51} \cdot \psi_{r\beta}(k) & -T_e \cdot a_{51} \cdot \psi_{r\alpha}(k) & 0 & 0 & 1 \\ 0 & 0 & 0 & 0 & 0 \end{bmatrix}$$

$a_{51} = \frac{n_{pp}^2.3.L_m}{2.J.L_r}$,

$$B_{d_6} = \begin{bmatrix} B_{d_5}^t & [0 \quad 0]^t \end{bmatrix}^t, \qquad C_6 = \begin{bmatrix} C_5 & [0 \quad 0]^t \end{bmatrix}$$

T_e is the sampling period, and J is the total moment of inertia referred to the motor shaft.

Note :
To simplify, it assumes that for each sampling period T_e, $\dot{\Gamma}_{load}$ = 0.

4.2. *IRFOC θ_e estimation using slipping angle velocity ω_{sl}*

In the case of the indirect method, the transformation angle is determined from ω_{sl}, as shown in the equation (5) below :

$$\omega_e - \omega_r = \omega_{sl} = (\frac{1}{\tau_r}) \cdot \frac{i_{sq_{ref}}}{i_{sd_{ref}}} \tag{5}$$

with

$$\theta_e = \int_0^T \omega_e \, \mathrm{d}t + \theta_e(0) \tag{6}$$

It is assumed that at the start, for the IM, rotor flux is null, and thus : $\theta_e(0)$ = 0.

$$\theta_e = \int_0^T (\frac{1}{\tau_r} \cdot \frac{i_{sq_{ref}}}{i_{sd_{ref}}} + \omega_r)\mathrm{d}t \tag{7}$$

4.3. *Comparison between DRFOC and IRFOC under nominal conditions*

In this section, the direct and indirect RFOC methods are compared under standard operating conditions. For DRFOC and IRFOC, the control is speed sensorless. Both approaches are commonly used in the control of induction motors, each offering unique advantages and trade-offs. From an implementation perspective, the DRFOC method is more complex, primarily due to the integration of the EKF observer, whose coefficients determination often relies on an empirical trial-and-error approach, requiring a methodical and rigorous process. The control schematic for the simulation is shown in Figure 4.

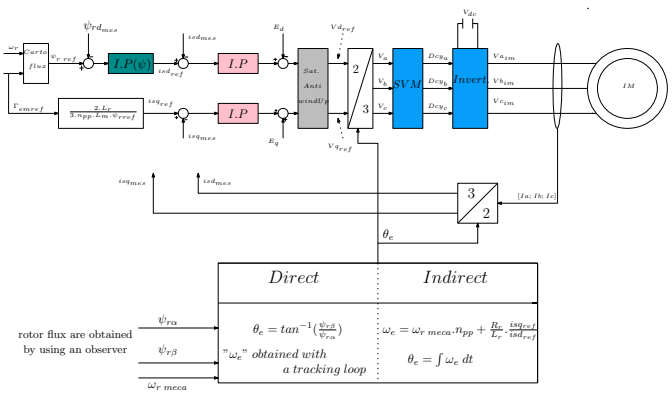

Figure 4. Blog diagram of IRFOC and DRFOC.

The PI controllers used for both the internal (current) and external (flux) regulation are tuned using the pole placement method. The reference flux is obtained from a Look-Up Table (LUT) provided by the industry partner (SAFRAN). Several operating points (Figure 2) defined based the maximum torque Γ_{max} and the maximum speed $\omega_{r_{max}}$ are tested (τ_{r_5}%(curr)=10ms).
Performance analysis of the two torque control methods reveals that, under identical control conditions, the indirect method demonstrates superior results. Specifically, this method exhibits fewer torque oscillations at high speeds. Under nominal operating conditions, both control strategies offer similar performance in terms of the transient response of the actual torque (Figure 5).

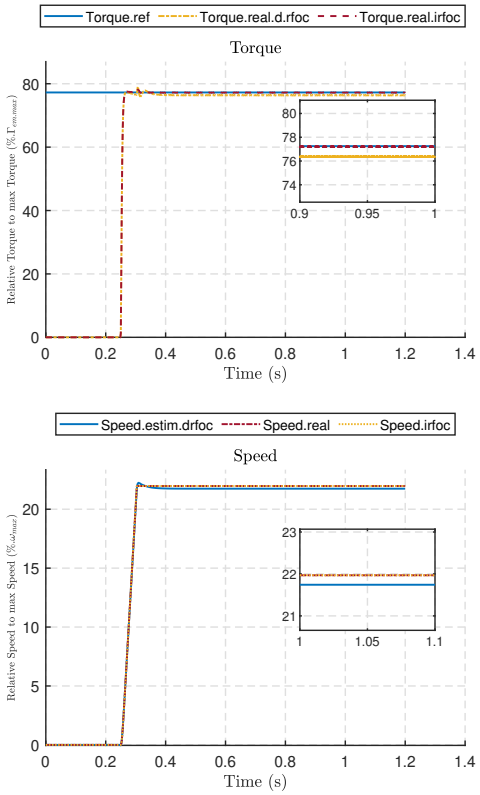

Figure 5. Comparison of Torque and Speed (simulation point P3)

5. IMPACT OF PARAMETER VARIATIONS ON THE PRODUCED TORQUE IN THE IRFOC STRATEGY

5.1. Analytical study

This study aims to analyze the influence of parameter variations on the performance of the torque control system.
These studies focus on the IRFOC method, starting from the previous equation (7).

Assumption 1 *unsaturated machine*

Assumption 2 *fast and accurate flux control :*

$$\psi_{rd_{mes}} = L_m \cdot i_{sd_{mes}}, \qquad \psi_{rd_{real}} = L_{m_{real}} \cdot i_{sd_{real}} \tag{8}$$

Assumption 3 *ideal regulator :*

$$i_{sdq_{ref}} = i_{sdq_{mes}}, \qquad \psi_{rd_{ref}} = \psi_{rd_{mes}} \tag{9}$$

Assumption 4 $L_r = L_m$

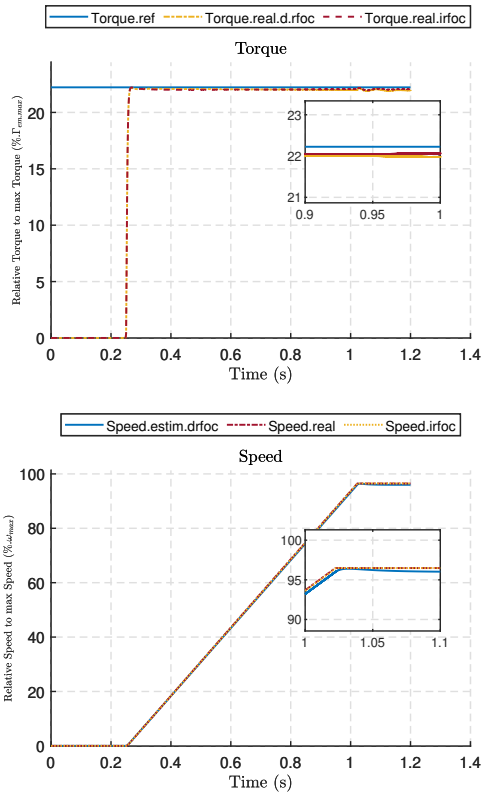

Figure 6. Torque and Speed at the Simulation Point P6

In this paper [8], authors provide the following relation (10) between $\theta_{e_{err}} = \theta_{e_{estim}} - \theta_{e_{real}}$ and rotor parameters.

$$\theta_{e_{err}} = \arctan\left(\frac{\frac{1}{\tau_r} - \frac{1}{\tau_{r_{real}}}}{\frac{1}{\tau_r}\cdot\frac{i_{sq_{mes}}}{i_{sd_{mes}}} + \frac{1}{\tau_{r_{real}}}\cdot\frac{i_{sd_{mes}}}{i_{sq_{mes}}}}\right) \tag{10}$$

x_{real} corresponds to the actual parameters, and for our case, $\frac{L_m}{L_{lr}} \approx 1000$, thus $L_r \approx L_m$. $L_r = L_m + L_{lr}$, where L_{lr} is the leakage inductance. Assumption 4 is verified for the case under study since $\frac{L_m}{L_{lr}} \approx 1000$.
Now let us define x = $L_m/L_{m_{real}}$.

$$\theta_{e_{err}} = \arctan\left(\frac{\frac{R_r}{R_{r_{real}}}(2-x) - 1}{\frac{R_r}{R_{r_{real}}}(2-x).\frac{i_{sq_{mes}}}{i_{sd_{mes}}} - \frac{i_{sd_{mes}}}{i_{sq_{mes}}}}\right) \tag{11}$$

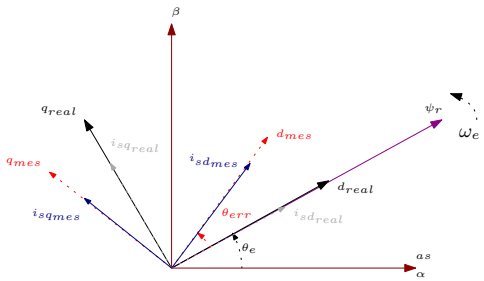

Figure 7. Impact of the deviation of the dq frame on the currents i_{sd} and i_{sq}

From the vectorial representation in Figure (7), it follows that :

$$\begin{cases} i_{sd_{real}} = i_{sd_{mes}}.cos(\theta_{e_{err}}) - i_{sq_{mes}}.sin(\theta_{e_{err}}) \\ i_{sq_{real}} = i_{sd_{mes}}.sin(\theta_{e_{err}}) + i_{sq_{mes}}.cos(\theta_{e_{err}}) \end{cases} \tag{12}$$

From Assumption 2, Eq. 8 :

The expression of $\Gamma_{em_{real}} = f(\theta_{err}, x)$:

$$\Gamma_{em_{real}} = \frac{3}{2} \cdot n_{pp} \cdot \frac{L_{m_{real}}}{L_{r_{real}}} \cdot (\psi_{rd_{real}} \cdot i_{sq_{real}}) = \frac{3}{2} \cdot n_{pp} \cdot \frac{L^2_{m_{real}}}{L_{r_{real}}} \cdot i_{sd_{real}} \cdot i_{sq_{real}}$$

$$\Gamma_{em_{real}} = \frac{3}{2} \cdot n_{pp} \cdot \frac{L^2_{m_{real}}}{L_{r_{real}}} \cdot [i_{sd_{mes}} \cos(\theta_{e_{err}}) - i_{sq_{mes}} \sin(\theta_{e_{err}})] \cdot [i_{sd_{mes}} \sin(\theta_{e_{err}}) + i_{sq_{mes}} \cos(\theta_{e_{err}})]$$

$L_r = L_m$, previous equation becomes :

$$\Gamma_{em_{real}} = \Gamma_{em_{mes}} \frac{1}{x}[cos^2(\theta_{e_{err}}) - sin^2(\theta_{e_{err}})] + \frac{3}{2} n_{pp} \frac{L_m}{x} sin(\theta_{e_{err}}) cos(\theta_{e_{err}}).(i^2_{sd_{mes}} - i^2_{sq_{mes}}) \quad (13)$$

With $\Gamma_{em_{real}}$ and $\Gamma_{em_{estim}}$ corresponds respectively to the real electromagnetic torque provided by the IM and the estimated one.
The formula (13) introduces a new development that has not been presented previously, offering an innovative approach to the analytical study of the accuracy of the real torque generated by the motor under parameter variations. This formula enables us to estimate the deviation between the actual torque generated by the motor and the reference torque. By taking into account the known maximum and minimum variations in both the L_m and R_r, one can predict the resulting torque error more accurately and assess the robustness of the control strategy.

5.2. *Simulation Results*

In Figure 8, the error in θ_e is plotted as a function of the variation in R_r on the x-axis and the variation in L_m on the y-axis. This allows us to observe how changes in these parameters affect the accuracy of the transformation angle.

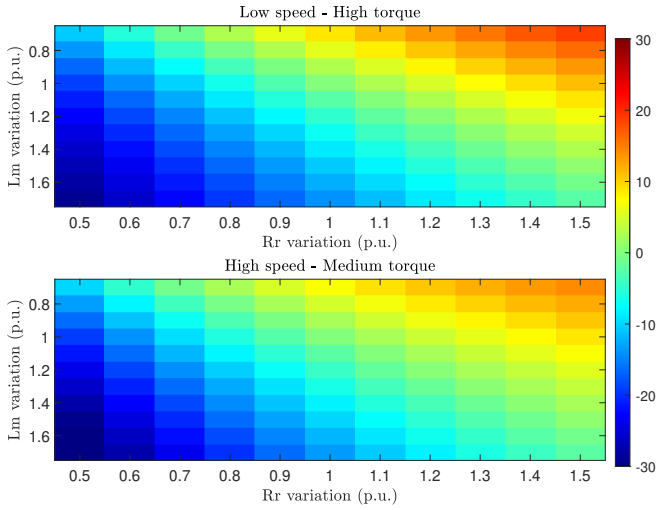

Figure 8. $\theta_{err}(°)$ variation according to the operating point and parameter variations

In Figure 9, the same principle is applied using the expanded formula previously presented (eq. 13).

Instead of observing the error in the transformation angle, the error in torque is plotted. In this case, the torque error is represented as a function of the variation of R_r on the x-axis and the variation of L_m on the y-axis. This figure allows us to analyze how changes in these two parameters influence the accuracy of the torque generated by the motor.

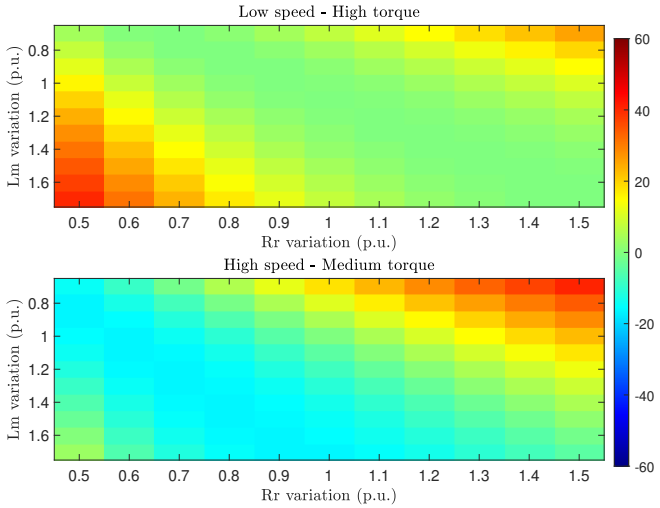

Figure 9. Relative Torque error (%) variation according to the operating point and parameter variations

Based on these mappings, it can be observed that the angle error (θ_{err}) can be either negative or positive. When the mutual inductance is increasingly underestimated and the rotor resistance overestimated in the control part (Figure 8), this tends to cause a positive angle error, specially in cases of machine saturation and overheating. Conversely, when the mutual inductance is overestimated and the rotor resistance is underestimated, a negative angle error typically occurs. In other scenarios, different from the two mentioned above, the angle varies non-monotonically with changes in the $L_m/L_{m_{real}}$ and $R_r/R_{r_{real}}$ ratio.
In consequence, considering typical parameter variation ranges, a torque variation between approximately -40% and 50% (Figure 9) can be observed, regardless of the operating point and parameter variation.
In summary, it has been found that there is no monotonically increasing relationship between the error in the transformation angle and the error in the torque caused by parameter variations. For instance, at point P8, an increase in $\theta_{e_{err}}$ leads to decrease the error on the produced torque. Similarly, at points P1, P3, and P6, a negative (respectively positive) $\theta_{e_{err}}$ does not necessarily result in a negative (respectively positive) torque error. This analysis also shows that it is possible to achieve zero torque error while still having an error in θ_e. Therefore, it provides a more comprehensive understanding of the impact of parameter variations on the accuracy of the produced torque within the context of IRFOC.

6. COMPARING THE ROBUSTNESS OF DRFOC AND IRFOC

In this section, the robustness of the two control techniques (DRFOC and IRFOC) as a function of R_r and L_m variation is evaluated. It should be noted that, due to confidentiality reasons, the parameter values are not disclosed.
For robustness tests, the IRFOC control is not robust to the variation of R_r (Figure 10) or to the variation of L_m (Figure 11). The variation of R_r as a ratio is plotted as a function of the error in the real torque developed by the machine, and the results obtained through simulation are consistent with those predicted in the theoretical studies (Figure 9) with (13). It is evident that the

use of a flux observer in the DRFOC strategy greatly reduces the negative impact of parameter errors, particularly in the presence of variations in R_r and L_m. Owing to the robustness of the EKF, DRFOC maintains a very low torque error across a wide range of parameter deviations, making it well-suited for environments where such variations are inevitable or cannot be precisely controlled.
In contrast, under nominal operating conditions, where the parameters are assumed to be well identified and stable, the IRFOC approach proves to be more accurate and efficient. However, at low speeds, sensorless DRFOC may suffer from reduced observability, limiting its accuracy despite its robustness.
In conclusion, IRFOC excels in nominal, well-characterized scenarios, whereas observers used in the DRFOC offers greater resilience to parameter uncertainties. These complementary strengths underline the potential benefit of a hybrid control approach that dynamically combines the accuracy of IRFOC with the robustness of DRFOC, ultimately aiming to achieve a more adaptive and fault-tolerant control system.

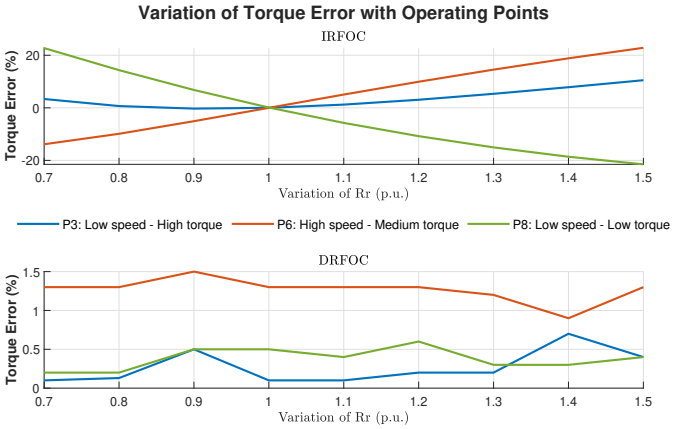

Figure 10. Variation of Torque Error as a function of R_r accuracy

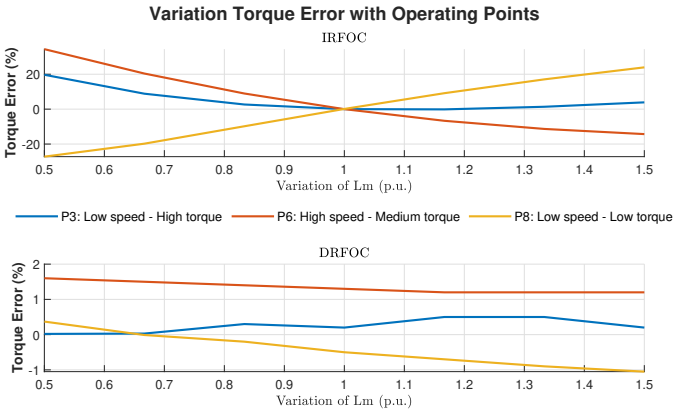

Figure 11. Variation of Torque Error as a function of L_m accuracy

7. CONCLUSION

This study presents a comparison between DRFOC and IRFOC in torque control under parametric variations, representing realistic application scenarios. The analytical investigation offers deeper insights into how parameter variations influence the accuracy of the torque control within the IRFOC framework.
In summary, IRFOC proves highly effective under nominal conditions where system parameters are well known and stable. In contrast, the DRFOC strategy demonstrates strong robustness in the face of parameter uncertainties, primarily due to the use of a flux observer such as the EKF, which helps compensate for inaccuracies in motor parameters like R_r and L_m. However, this robustness comes with a trade-off: sensorless DRFOC may suffer from observability issues, particularly at low speeds where the absence of a speed sensor limits the quality of state estimation. These complementary characteristics highlight the relevance of developing in the future a hybrid control strategy that takes advantage of the precision of IRFOC in stable conditions and the adaptability of DRFOC under parameter variations, thus aiming for a more reliable and versatile control system.

8. ACKNOWLEDGMENTS

Gratitude is expressed to French ANRT and Safran Group for funding this research, which made the completion of this work possible. Special thanks are also extended to colleagues from Safran Ventilation Systems and Safran Landing Systems for their constructive feedback, technical support, and the resources they provided.

9. REFERENCES

[1] K. Ebner, A. Habersetzer and A. Seitz, "Aircraft Electrification – System-Level Potentials for Aviation Decarbonization," 2022 24th European Conference on Power Electronics and Applications (EPE'22 ECCE Europe), Hanover, Germany, 2022, pp. P.1-P.1.

[2] B. Sarlioglu and C. T. Morris, "More Electric Aircraft: Review, Challenges, and Opportunities for Commercial Transport Aircraft," in IEEE Transactions on Transportation Electrification, vol. 1, no. 1, pp. 54-64, June 2015

[3] J. Chen, C. Wang and J. Chen, "Investigation on the Selection of Electric Power System Architecture for Future More Electric Aircraft," in IEEE Transactions on Transportation Electrification, vol. 4, no. 2, pp. 563-576, June 2018

[4] Joachim Bocker and Shashidhar Mathapati. State of the art of induction motor control. In 2007 IEEE International Electric Machines Drives Conference, volume 2, pages 1459–1464, 2007.

[5] M. Depenbrock. Direct self-control (dsc) of inverter-fed induction machine. IEEE Transactions on Power Electronics, 3(4) :420–429, 1988

[6] Kuczmann, M., Horváth, K. (2024). Tensor Product Alternatives for Nonlinear Field-Oriented Control of Induction Machines. Electronics, 13(7), 1405.

[7] Sang-HooN Kim. Electric motor control dc, ac and bldc motors. In Electric Motor Control, 2017

[8] Yang Liu, Geng Tao, Huai Wang, and Frede Blaabjerg. Analysis of indirect rotor field oriented control-based induction machine performance under inaccurate field- oriented condition. In IECON 2017 - 43rd Annual Conference of the IEEE Industrial Electronics Society, pages 1810–1815, 2017

[9] G. Özkurt and E. Zerdali, "Design and Implementation of Hybrid Adaptive Extended Kalman Filter for State Estimation of Induction Motor," in IEEE Transactions on Instrumentation and Measurement, vol. 71, pp. 1-12, 2022, Art no. 7500212

[10] Qijun Xia, Ming Rao, Yiqun Ying, Xuemin Shen,Adaptive fading Kalman filter with an application, Automatica, Volume 30, Issue 8, 1994,Pages 1333-1338

[11] E. Zerdali, "A Comparative Study on Adaptive EKF Observers for State and Parameter Estimation of Induction Motor," in IEEE Transactions on Energy Conversion, vol. 35, no. 3, pp. 1443-1452, Sept. 2020